

# Qualification of Laser-Based Powder Bed Fusion of Metals (PBF-LB/M) Using Scanner Data

Jesus Rivas<sup>a</sup> Jorge Mireles<sup>a, b</sup> Francisco Medina<sup>a, b</sup>

<sup>a</sup> *W.M. Keck Center for 3D Innovation, The University of Texas at El Paso, El Paso, TX 79968, USA.*

<sup>b</sup> *Department of Aerospace and Mechanical Engineering, The University of Texas at El Paso, El Paso, TX 79968, US*

## Abstract

Laser-based powder bed fusion of metals (PBF-LB/M) enables the manufacture of complex geometries for high-performance applications. However, process variations can lead to dimensional inaccuracies or microstructural issues affecting the overall part quality. In consequence, there is a need for efficient qualification methods to ensure part consistency, reliability, and reproducibility. The proposed qualification approach leverages key scanning system data to simulate the process at both micro- and macro-scales. The method aims to enhance analytical models to simulate melt pool morphology by incorporating scanning data containing speed, acceleration, deceleration, and default process scanning parameters such as polygon delays. In addition, the method uses laser beam positions to simulate geometry outcomes for macro-scale qualification approaches. By using more representative speed profiles and actual laser paths, the proposed method offers a practical and efficient strategy, improving accuracy and confidence in process qualification.

## 1.0 Introduction

Laser-Based Powder Bed Fusion of Metals (PBF-LB/M) enables the manufacture of complex components for high-performance applications.<sup>1</sup> The process can produce multiple geometries, such as those used for aerospace components, heat exchangers, and biomedical implants with specific performance outcomes, including lightweight strength or energy absorption.<sup>2-4</sup> PBF-LB/M process variations resulting in dimensional, microstructural, and surface roughness deviations impact the overall part quality, limiting the adoption in industry applications.<sup>5,6</sup> In consequence, there is a need for efficient qualification methods to ensure part consistency, reliability, and reproducibility.<sup>7,8</sup> Some qualifications process relies on test coupons, destructive testing, and geometry inspections to ensure the part quality. As part of qualifications and process understanding efforts, multiple authors have been reviewing process outcomes either in a micro-scale approach, for example, evaluating melt pool morphology, or in a macro-scale, reviewing geometry accuracy, surface quality, or porosity.<sup>9</sup> However, current studies underestimate the complex speed and path profiles variations from commanded targets, limiting the accuracy of the qualification process. In response, this study proposes the integration of scan data logs into micro and macro evaluations to improve qualification accuracy.

Micro-scale evaluations focusing on melt pool size and shape are crucial in process qualification approaches, since they can be correlated with process windows and part properties such as density, hardness, microstructure, and other mechanical characteristics.<sup>10-12</sup> Li et al. 2024 evaluated the effect of melt pool morphology and grain structures of alloy 718 samples and found

a correlation between melt pool shapes and hardness values.<sup>13</sup> Similarly, melt pool evaluations help to determine optimal process windows by defining conduction and keyhole modes, which contribute to the overall part quality.<sup>14</sup>

Numerical and analytical models have been developed to simulate the PBF-LB/M process in a micro-scale qualification approach. Numerical models are highly accurate in predicting melt pool physics and morphology; however, they are associated with a large computational cost, a single-track study using scan speed and laser spot can take at least several hours, which makes them impractical, as reported by Parivendhan et al. 2023 and Bayat et al. 2019.<sup>15,16</sup> In contrast, the analytical or semi-analytical approach based on deposited energy has been used to describe melt pool morphology; however, this relation is insufficient to describe the melt pool behavior.<sup>17</sup> More advanced analytical models using the normalized enthalpy, a dimensionless variable combining power, speed, and thermophysical properties of the material, have been studied by several authors.<sup>18</sup> Coen et al. 2022 proposed a methodology combining semi-analytical expressions of the melt pool width and depth and the aspect ratio, defining the conduction and keyhole melting regimes with good agreement between the experimental and model data.<sup>19</sup> One limitation of published studies when evaluating melt pool morphology is diminishing the speed variations from acceleration, deceleration, or parameter configurations, such as polygon or mark delay of the scanning system. It is well documented that the scanning system can induce defects such as porosity related to speed and scanning delays. Even nominal speed may not be achieved in some scanning and geometry configurations.<sup>20</sup> Thus, employing accurate speed profiles in melt pool simulations can enhance the qualification approaches.

As previously described, macro-scale evaluation in terms of geometry accuracy is another important qualification metric, sensitive to process parameter variations.<sup>21-24</sup> The deviation between the intended geometry and the produced geometry significantly impacts mechanical performance, functionality, and reliability. For example, deviations in the strut thickness of lattice structures reduce the compressive strength. Similarly, surface irregularities can reduce fatigue or lead to stress concentration points. Dimensional inaccuracies can shift lattice structures from intended stretch-dominated (high stiffness and strength) to unintended bending-dominated behavior (lower strength, higher compliance).<sup>25-32</sup> Macro-scale part qualification using X-ray Computed Tomography (XCT) provides pore distribution and can quantify deviation from the original Computer Aided Design (CAD) model.<sup>33</sup> This method is the gold standard for complex internal geometries; however, ongoing work continues to refine scanning protocols, segmentation algorithms, and best practices to ensure reliability and repeatability.<sup>34-40</sup> Other methods to quantify geometry outcomes include Scanning Electron Microscopy (SEM) to evaluate surface morphology and structural deviations at the microscale or Finite Element Analysis (FEA) to evaluate thermal distortions that significantly contribute to geometric inaccuracies.<sup>41-43</sup> However, challenges remain associated with developing methods that balance cost-effectiveness, practical applicability, and measurement accuracy.<sup>44</sup>

In response to some of the limitations when assessing process qualifications, this study objective is to integrate scanning data with accurate speed profiles, including acceleration and deceleration phases into analytical models to have a more accurate process qualification results. In addition, the research introduces the use of laser position data to simulate geometry profiles for macro-scale qualification approaches.

## 2.0 Methodology

Micro and Macro-scale qualification approaches were integrated into process scanning data to improve process qualification accuracy, See Figure 1. A micro-scale method was simulated by adapting scanning paths and speed profiles into a first-order analytical model for melt pool width estimation. Process data containing actual scan paths were collected using a custom device installed in an EOS M290 with details in section 2.1. Speed profiles were calculated for each vector segment using the scanned data positions and the sampling time rate, (see section 2.2). The simulated melt pools widths were validated through experimental data to estimate the model accuracy under different scanning paths, (see section 3.0). Data-driven model simulations were obtained using laser path positions and the melt pool width for a macro-scale qualification by Finite Element Analysis with details described in section 3.1.

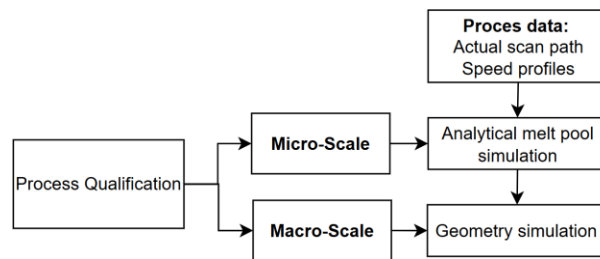


*Figure 1 Micro and macro scale process qualification using scan path and speed profiles.*

### 2.1 Process Data Collection

The PBF-LB/M process relies on precise control of a laser beam, guided by a galvanometric scanning system. The scan control systems consist of galvo motors, driven by digital-to-analog control systems that execute scanning paths through a closed-loop feedback mechanism. An external high-speed data acquisition system, developed by Tailored Alloys, was installed in the EOS machine to simultaneously capture the commanded position sent to the galvo driver and the actual feedback positions reached by the galvo encoder. This method enables the data collection of the laser path (commanded and actual positions of scanning paths). The scanned geometry consisted of multiple shapes containing angled geometries, circular shapes, and irregular shapes to evaluate multiple scan paths, see Figure 2.

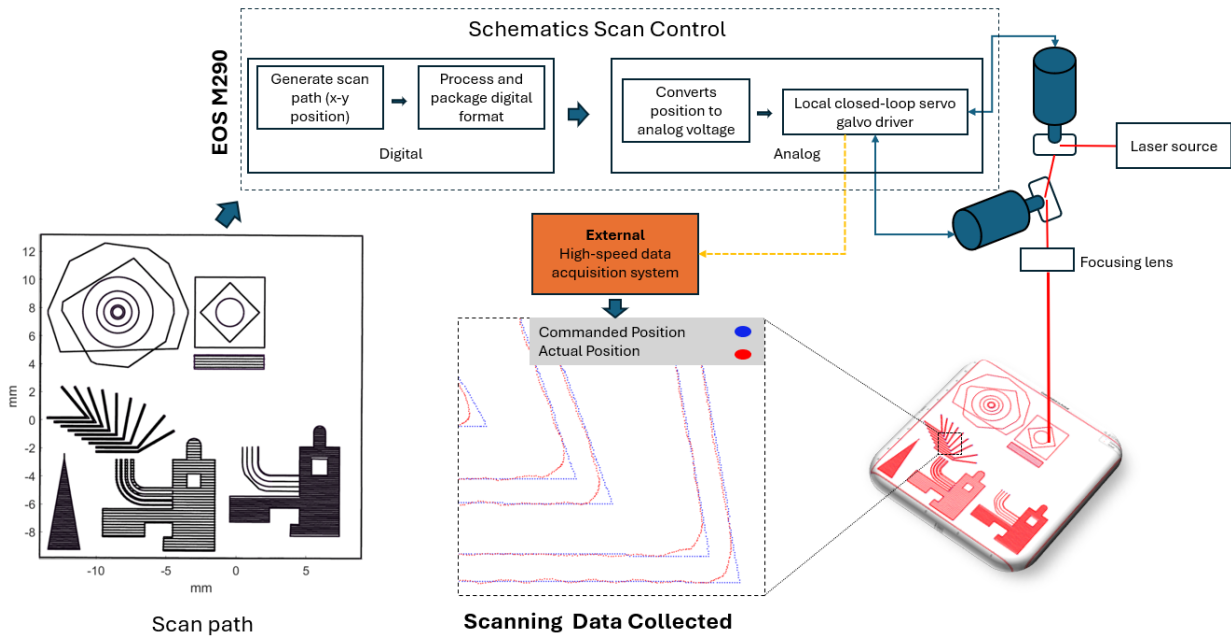


Figure 2 Process data collection method. The controller generates the  $x$ - $y$  scan path, packages it in digital form, converts it to analog drive voltages, and sends them to a local closed-loop galvanometer driver then an external high-speed acquisition system (orange) records the commanded and actual feedback signals.

## 2.2 Data Pre-Processing Calculation of Speed Profiles

The actual  $X$  and  $Y$  laser's position of each scanning path is recorded at intervals of  $10 \mu\text{s}$  (100 kHz clock rate), and the difference in position between two consecutive time steps is employed to calculate the laser beam speed with the following Equation 1.

Equation 1

$$v(t) = \frac{\sqrt{(X(t+1) - X(t))^2 + (Y(t+1) - Y(t))^2}}{\Delta t}$$

Where:

- $v(t)$  is the speed at the time  $t$ .
- $X(t+1)$  and  $X(t)$  are the positions at times  $t+1$  and  $t$  along the X-axis.
- $Y(t+1)$  and  $Y(t)$  are the positions at times  $t+1$  and  $t$  along the Y-axis.
- $\Delta t$  is the time difference between two consecutive measurements.

## 2.3 Analytical Melt Pool Simulation Approach

A conduction-based square root relationship between the power and speed ratio from Rosenthal-type conduction solutions offers a first-order approximation of the melt pool width. This analytical melt pool width simulation, defined by equation (2), uses a constant  $\varepsilon$  that consolidates material properties (e.g., thermal conductivity, density, heat capacity, melting temperature) and process factors (e.g., absorptivity, radiation, convection, etc.). While this first-order method does

not consider complex phenomena such as recoil pressure, Marangoni flow, or keyhole formations, it was used as a conservative approach to evaluate the integration of speed profiles obtained from scanning data into analytical models. To estimate the value of the constant  $\varepsilon$  that consolidates material properties and process factors, a regression model was used. In addition, MAE (Mean Absolute Error), RMSE (Root Mean Squared Error), and  $R^2$  (Coefficient of Determination) were calculated to evaluate the performance and validity of the analytical model in comparison with experimental data.

Equation 2

$$Wm = \varepsilon \sqrt{\frac{P}{v}}$$

Where:

$\varepsilon$  – Consolidates material properties and process factors.

$P$  -Laser power

$v$  -Speed

$Wm$  – Melt pool width/Scan line width

### 3 Experimental Validation and Results

A scanning plate approach was used to isolate the scanner path from powder interaction. The plate was made of Stainless Steel 304 with a nominal dimension of 25x25x3.5mm and was in the center of the building platform. A laser power of 100W and 1000mm/s and 800 mm/s scanning speeds were tested in different geometries, see Figure 3. High-resolution imaging was obtained using a Keyence VHX-7000 4K microscope (Keyence Corporation, Osaka, Japan) with an accuracy of 0.001 mm and up to 500X magnification to measure the scan line/melt pool width ( $Wm$ ).

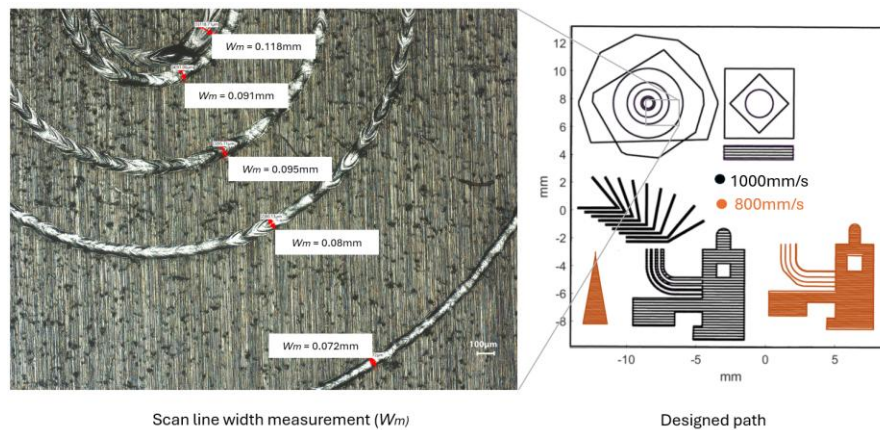


Figure 3 Scan line width measurement across multiple circular geometries where different line widths are observed for the same commanded speed.

Figure 4 shows the actual speed calculation based on the previous Equation (1) and the commanded speed (1000m/s). As observed, multiple regions show speed variations from commanded, especially in corners and circular shapes. These speed profiles were adapted to analytical models to simulate the melt pool width across the entire scan path regions.

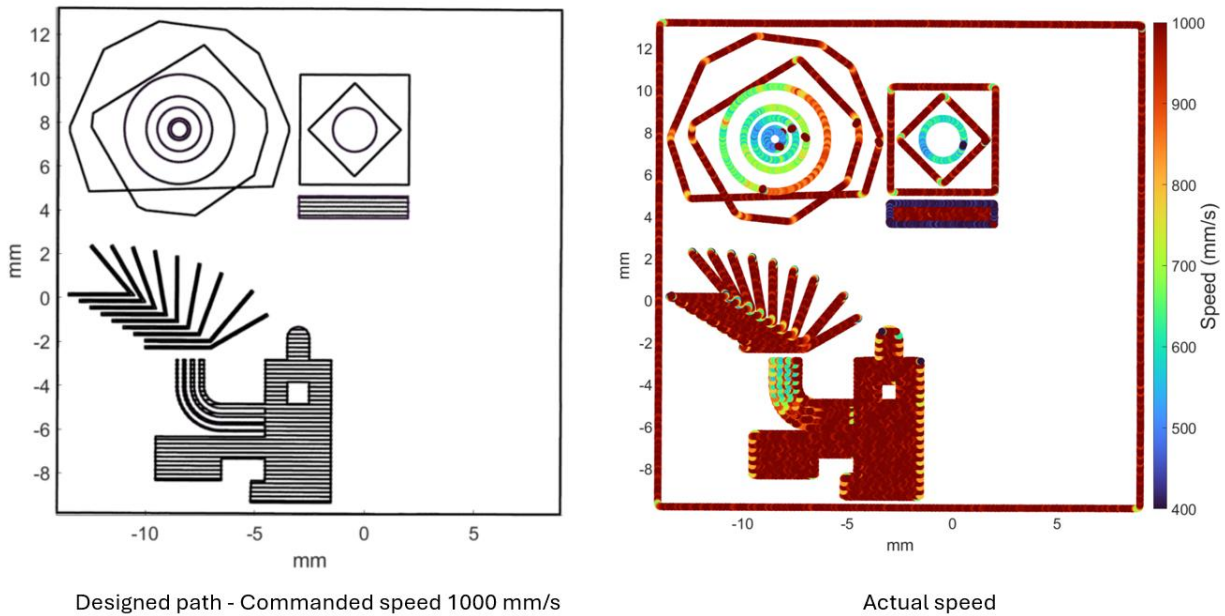


Figure 4 Commanded and actual speed at different scan path regions. The figure illustrates how the scan control introduce local variations under a single commanded speed.

Figure 5 shows the experimentally measured line width ( $W_m$ ) and the calculated speed at two scan path segments (straight and a circular path), where the commanded speed was set to 1000/mms. The scan line width measurement shows significant variations between the two segment paths, similar to the scan speed calculation obtained from the scan data, with almost 50% reduction from the commanded value at the circular shape. The result highlights the scanner systems' limitations and configurations in the scanning speed based on the geometry regarding the commanded set value. The results highlight the importance of integrating more accurate speed profiles when evaluating micro- and macro-scale regions, either with analytical or numerical models.

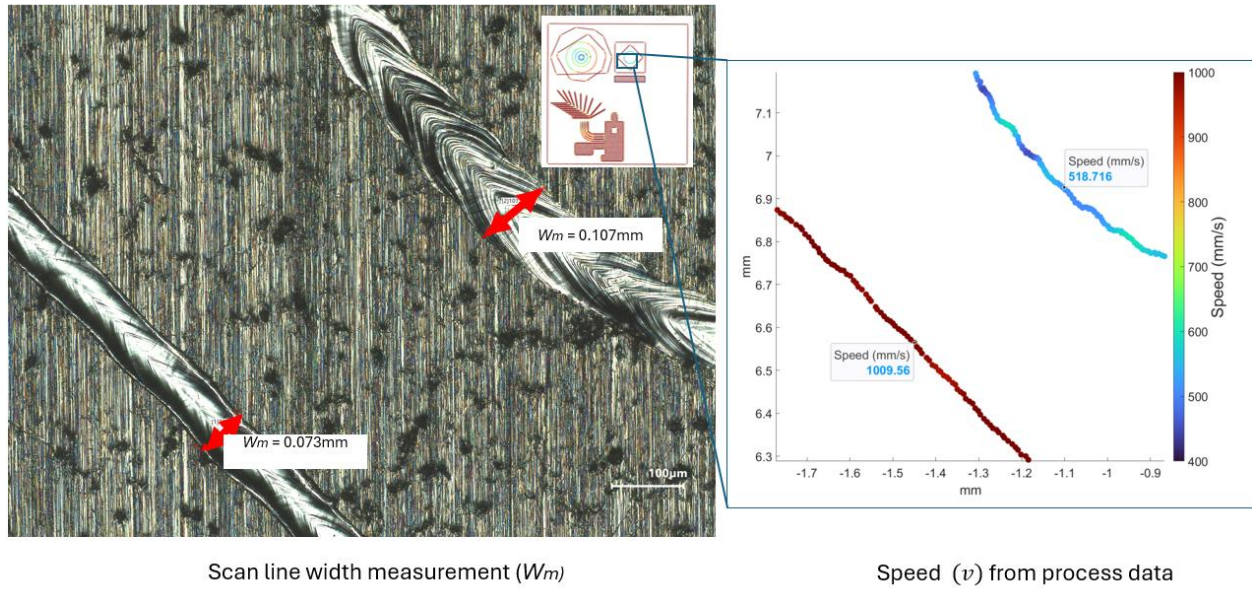
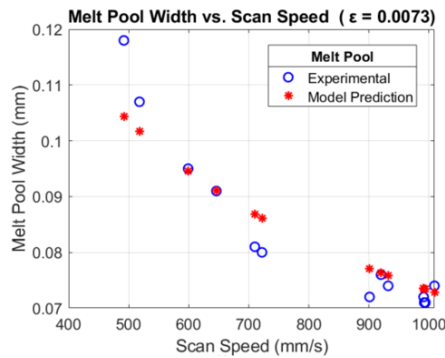


Figure 5 Line width and speed variations related to the geometric shape, both tracks were executed with the same commanded speed of 1000 mm/s, yet the actual speed locally dropped to ~520 mm/s for the wider track and stayed near 1000 mm/s for the narrower track.

Figure 6 illustrates the experimental and predicted melt pool widths across multiple scanning speed values, derived from the commanded speed (1000m/s). A calculated constant,  $\epsilon = 0.007321$ , was obtained from the regression model and the previous Equation (2), consolidating the material properties and process parameters of Stainless Steel 304. The regression model shows a Mean Absolute Error (MAE) of 0.0036 mm, a Root Mean Square Error (RMSE) of 0.0051 mm, and a coefficient of determination ( $R^2$ ) of 0.8799, which are acceptable values for a first-order simulation.



Comparison of Width measurement ( $W_m$ ) and predicted width

Figure 6 Melt pool width based on Experimental and predicted data.

Figure 7 illustrates the simulated melt pool width along the entire scan path. In addition to the observations from the previous Figure 5, variations in scanning speed significantly affect not only circular but also irregular paths, which both impact the scan path uniformity quality.

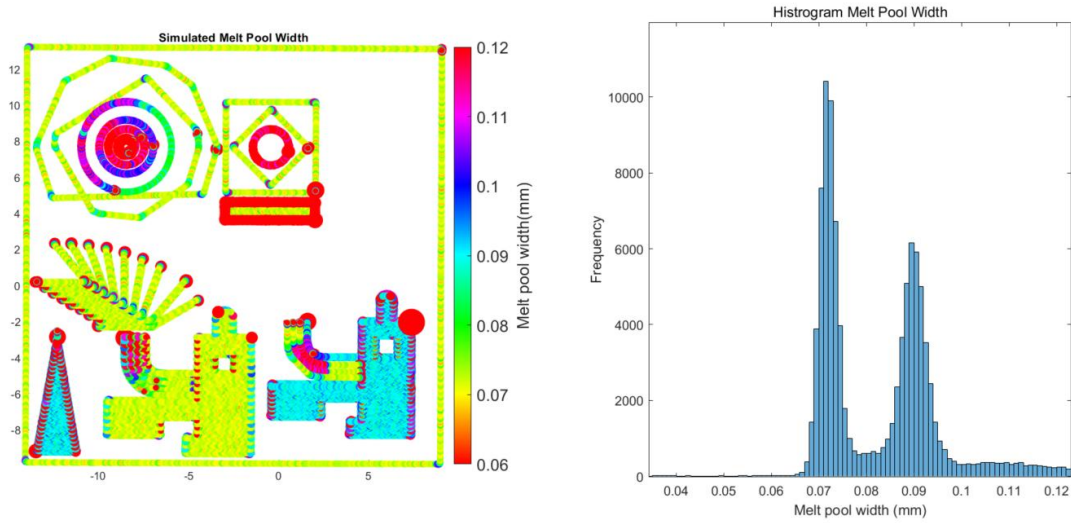


Figure 7 Melt pool width distribution across multiple scanning paths reflecting different speed regimes (steady straight scans, curved/accelerating regions, and dwell/overlap zones) that produce distinct energy input and, consequently, different melt-pool width.

The effect of scan vector length on melt pool width can be observed as well by incorporating scan data into the analytical model, see Figure 8. Differences in melt pool width between short and long vectors produce morphology variations related to excessive energy input as discussed by Li et al. (2024). The simulations also captured melt pool width variations at the start and end of scan vectors, as well as in corner regions, where deviations reached up to 71.43%. These results emphasize qualification opportunities using scan data to assess the discrepancies between commanded and actual speed profiles, demonstrating how certain regions are susceptible to localized energy density fluctuations that can compromise part quality and consistency.

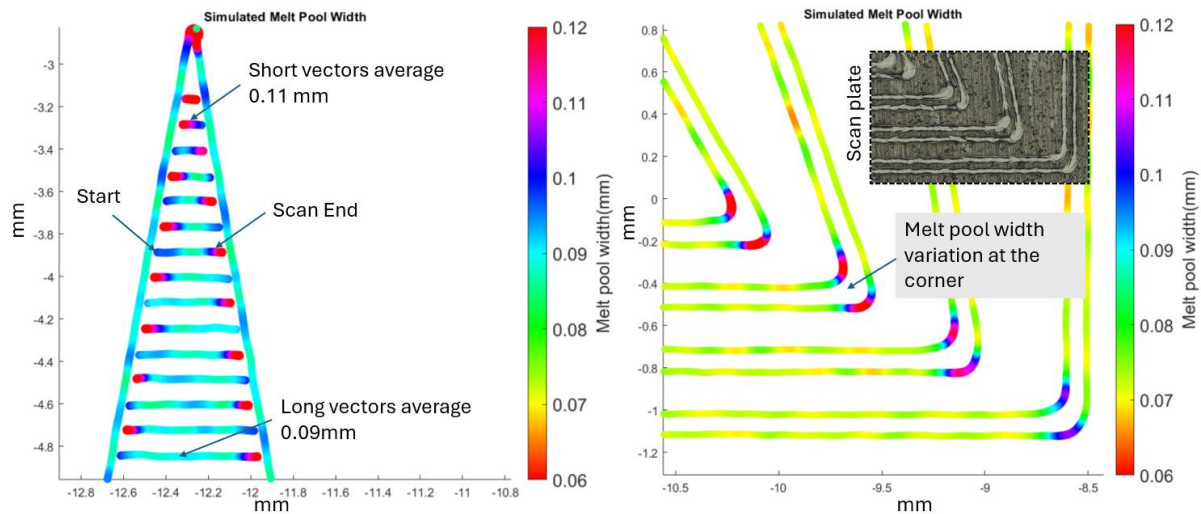


Figure 8 Impact of vector length and cornering on simulated melt-pool width (constant command 1000 mm/s).

### 3.1 Process-Driven Modeling Simulation

Figure 9 shows the process-driven modeling simulation of two circular paths obtained using scan data position and melt pool width simulations. For each discrete sample point along the scan trajectory, unit tangent and normal vectors were computed to accurately define local directions and offsets of the melt pool width. These vectors facilitated the creation of a closed polygon, representing the melt-pool's width outline at each segment. Delaunay triangulation was applied to convert these polygons into a structured mesh of triangles, enabling the representation of a continuous, accurately defined surface geometry. Finally, the generated triangular mesh was exported as a binary Standard Triangle Language (STL) file using MATLAB's built-in triangulation and export function (`stlwrite(triangulation(faces, vertices))`). The generated model provides a baseline for a more suitable geometric representation for further simulations and macro-scale qualifications.

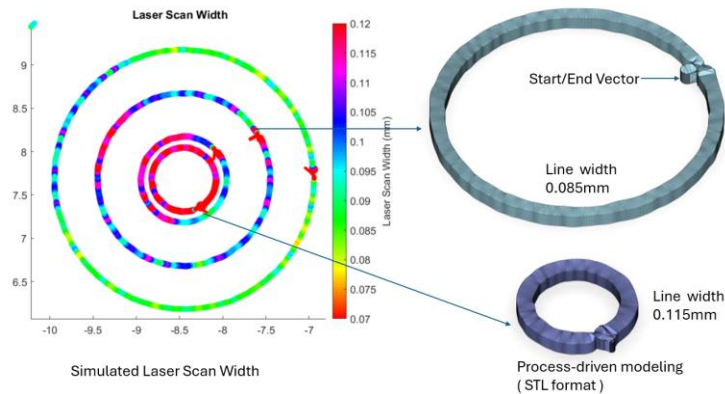


Figure 9 Process-driven modeling example using accurate paths and speed profiles.

Differences between Finite Element Analysis and the experimental results when performing mechanical evaluations in PBF-LB/M produced parts have been described by multiple authors, with special interest in small complex features such as those used in lattice structures. Process-induced defects, such as porosity or geometry variations, have been introduced into the Finite Element Models to improve the agreement between the simulation and experimental results. XCT data containing the process anomalies is typically used as a reference to induce defects into these models and improve the accuracy results.<sup>45,46</sup> Figure 10 shows a Finite Element Analysis of an angled segment (<5mm) focusing on the corner section using the designed or nominal geometry and process-driven geometry simulation described in the previous section. As shown, by using accurate process-driven scan paths and speed profiles, significant variations were observed between these two models. These results highlight the opportunities of scanning data induced defects into FEM to enhance the qualifications accuracy in a macro -scales approaches.

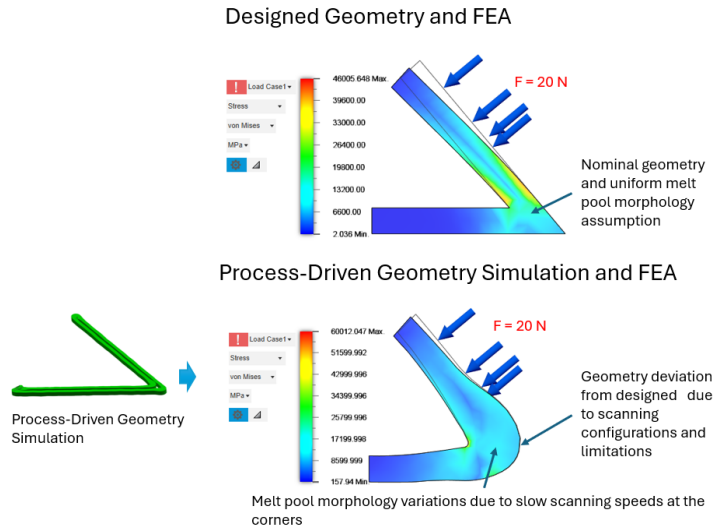


Figure 10 Comparison of the nominal and process design models used for the Finite Element analysis in a corner region.

## 4.0 Discussion

Scanning data has been used to characterize the overall performance of the scanning system and for calibration purposes, but not to correlate process defects such as porosity.<sup>47–49</sup> One advantage of evaluate scanner data is overcoming the unknown inner configuration and limitations of the scanning system, since many manufacturers do not provide access to these critical parameter configurations such as polygon delay, one of the key functions defining the scanner's influence on irregular geometries or mark delay another essential parameter, assigning the time required for the scanner system to switch between vectors that has been linked by researchers to porosity-related defects, such as keyhole formation.<sup>50,51</sup> Thus, the integration of scanning data and derived speed calculations can enhance part qualification by more accurately reflecting the thermal history and variations in melt pool morphology. The limitation of this qualification approach lies in the complex interaction between the laser scanning system and the powder bed, including factors such as powder uniformity, spatter particles, and other stochastic events, in consequence, these interactions must be accounted for to provide a more complete description of the (PBF-LB/M) process. Therefore, by coupling current in situ monitoring methods, such as optical, thermal, or acoustic techniques, with scanner data that includes scanning speed variations and positional information, process qualification can be enhanced and validated.

## 5.0 Conclusion and Future Work

In this study, scanning data has been collected with a custom device installed in an EOS machine. Scanner data positions were used to calculate speed profiles across multiple path geometries, including circles and angled paths. Experimental data was obtained by scanning the geometry in a Stainless-Steel plate without powder to isolate the scanner's behavior from other process interactions. The study used a correlation between speed and power and a constant factor that integrates material properties and process parameters to estimate the melt pool width. This method allows practical experimental evaluation of use of scan data integration in melt pool predictions and qualifications. A macro-scale qualification approach was proposed based on process-driven modeling, containing data positions and melt pool width.

Speed variations up to 50% from the commanded speed (1000m/s) in some geometries and path sections were found and highlight the importance of more representative scan speed profiles used for micro and macro-scale qualifications. Similarly, process-driven modeling containing representative speed profiles and scan paths could provide first-order models that can be used for Finite Element Analysis to improve mechanical performance predictions.

In conclusion, scanner data can be integrated into micro and macro qualification techniques and offers a practical and efficient strategy for improving accuracy and confidence in qualification methods. From an industry perspective, scan data qualification provides a low-cost process qualification technique that can be run without powder or coupons. Further work will be dedicated to the integration of scanner data with additional in-situ monitoring techniques, such as optical and thermal-based, and machine learning methods for enhanced process defect detection and prediction in micro and macro scale approaches.

## 6.0 Acknowledgements

The research described here was performed at The University of Texas at El Paso (UTEP) within the W.M. Keck Center for 3D Innovation (Keck Center). This material is based on research sponsored by Air Force Research Laboratory under Agreement Number FA8650-20-2-5700. The U.S. Government is authorized to reproduce and distribute reprints for Governmental purposes notwithstanding any copyright notation thereon. Additional support was provided by strategic investments via discretionary UTEP Keck Center funds and the Mr. and Mrs. MacIntosh Murchison Chair I in Engineering Endowment at UTEP. Disclaimer: The views and conclusions contained herein are those of the authors and should not be interpreted as necessarily representing the official policies or endorsements, either expressed or implied, of Air Force Research Laboratory or the U.S. Government.

## 7.0 References

1. Yadroitsev, I., Yadroitsava, I. & Du Plessis, A. *Basics of Laser Powder Bed Fusion. Fundamentals of Laser Powder Bed Fusion of Metals* (Elsevier Inc., 2021). doi:10.1016/b978-0-12-824090-8.00024-x.
2. Blakey-Milner, B. *et al.* Metal additive manufacturing in aerospace: A review. *Mater Des* **209**, 110008 (2021).
3. Kamal, M. & Rizza, G. *Design for Metal Additive Manufacturing for Aerospace Applications. Additive Manufacturing for the Aerospace Industry* (Elsevier Inc., 2019). doi:10.1016/B978-0-12-814062-8.00005-4.
4. Igor, S. *Aerospace Applications of the SLM Process of Functional and Functional Graded Metal Matrix Composites Based on NiCr Superalloys. Additive Manufacturing for the Aerospace Industry* vol. c (Elsevier Inc., 2019).
5. Russell, R. *et al.* *Qualification and Certification of Metal Additive Manufactured Hardware for Aerospace Applications. Additive Manufacturing for the Aerospace Industry* (Elsevier Inc., 2019). doi:10.1016/B978-0-12-814062-8.00003-0.

6. Dordlofva, Christo. *et al. Qualification Aspects in Design for Additive Manufacturing <em>A Study in the Space Industry</em>*.
7. Dowling, L., Kennedy, J., Shaughnessy, S. O. & Trimble, D. A review of critical repeatability and reproducibility issues in powder bed fusion. *Mater Des* **186**, 108346 (2020).
8. Gradl, P. R. *et al.* Geometric Feature Reproducibility for Laser Powder Bed Fusion (L-PBF) Additive Manufacturing with Inconel 718. *Addit Manuf* **47**, 102305 (2021).
9. Kim, F. H., Yeung, H. & Garboczi, E. J. Characterizing the effects of laser control in laser powder bed fusion on near-surface pore formation via combined analysis of in-situ melt pool monitoring and X-ray computed tomography☆. *Addit Manuf* **48**, 102372 (2021).
10. Yang, G. *et al.* Quality Control: Internal Defects Formation Mechanism of Selective Laser Melting Based on Laser-powder-melt Pool Interaction: A Review. *Chinese Journal of Mechanical Engineering: Additive Manufacturing Frontiers* **1**, 100037 (2022).
11. Li, E., Shen, H., Wang, L., Wang, G. & Zhou, Z. Laser shape variation influence on melt pool dynamics and solidification microstructure in laser powder bed fusion. *Additive Manufacturing Letters* **6**, 100141 (2023).
12. Wang, J., Zhu, R., Liu, Y. & Zhang, L. Understanding melt pool characteristics in laser powder bed fusion: An overview of single- and multi-track melt pools for process optimization. *Advanced Powder Materials* **2**, (2023).
13. Li, L., Chen, H., Wang, X. & Liao, Z. Effects of vector length on the melt pool morphology and grain structure characteristics of Alloy 718 in laser powder bed fusion. *J Mater Process Technol* **326**, (2024).
14. Tenbrock, C. *et al.* Influence of keyhole and conduction mode melting for top-hat shaped beam profiles in laser powder bed fusion. *J Mater Process Technol* **278**, 116514 (2020).
15. Parivendhan, G. *et al.* A numerical study of processing parameters and their effect on the melt-track profile in Laser Powder Bed Fusion processes. *Addit Manuf* **67**, 103482 (2023).
16. Bayat, M. *et al.* Keyhole-induced porosities in Laser-based Powder Bed Fusion (L-PBF) of Ti6Al4V: High-fidelity modelling and experimental validation. *Addit Manuf* **30**, 100835 (2019).
17. Scipioni Bertoli, U., Wolfer, A. J., Matthews, M. J., Delplanque, J. P. R. & Schoenung, J. M. On the limitations of Volumetric Energy Density as a design parameter for Selective Laser Melting. *Mater Des* **113**, 331–340 (2017).
18. Hann, D. B., Iammi, J. & Folkes, J. A simple methodology for predicting laser-weld properties from material and laser parameters. *J Phys D Appl Phys* **44**, (2011).

19. Coen, V., Goossens, L. & Hooreweder, B. Van. Methodology and experimental validation of analytical melt pool models for laser powder bed fusion. *J Mater Process Technol* **304**, 117547 (2022).
20. Pothen, M., Winands, K. & Klocke, F. Compensation of scanner based inertia for laser structuring processes. *J Laser Appl* **29**, (2017).
21. Leirmo, T. L. & Semeniuta, O. Investigating the Dimensional and Geometric Accuracy of Laser-Based Powder Bed Fusion of PA2200 (PA12): Experiment Design and Execution. *Applied Sciences* **11**, 2031 (2021).
22. Krasniqi, M. & Löffler, F. Dimensional accuracy of additively manufactured AlSi10Mg parts: Study of the influence of build platform position, process parameters and repeatability. 2–5 (2023).
23. Calignano, F., Lorusso, M., Pakkanen, J., Trevisan, F. & Ambrosio, E. P. Investigation of accuracy and dimensional limits of part produced in aluminum alloy by selective laser melting. *The International Journal of Advanced Manufacturing Technology* 451–458 (2017) doi:10.1007/s00170-016-8788-9.
24. Secondary, C. A. *et al.* Progress in Additive Manufacturing Measurement systems analysis for Beam Compensation , Scaling factors and Geometric Dimensioning for a metallic additively manufactured test artifact.
25. Liu, L., Kamm, P., García-Moreno, F., Banhart, J. & Pasini, D. Elastic and failure response of imperfect three-dimensional metallic lattices: the role of geometric defects induced by Selective Laser Melting. *J Mech Phys Solids* **107**, 160–184 (2017).
26. Mirzaali, M. J., Azarniya, A., Sovizi, S., Zhou, J. & Zadpoor, A. A. *Lattice Structures Made by Laser Powder Bed Fusion. Fundamentals of Laser Powder Bed Fusion of Metals* (Elsevier Inc., 2021). doi:10.1016/b978-0-12-824090-8.00020-2.
27. Echeta, I., Feng, X., Dutton, B., Leach, R. & Piano, S. Review of defects in lattice structures manufactured by powder bed fusion. *International Journal of Advanced Manufacturing Technology* **106**, 2649–2668 (2020).
28. Vrána, R. *et al.* Deviations of the SLM Produced Lattice Structures and Their Influence on Mechanical Properties. *Materials* **15**, 1–20 (2022).
29. Mazur, M. *et al.* *Mechanical Properties of Ti6Al4V and AlSi12Mg Lattice Structures Manufactured by Selective Laser Melting (SLM). Laser Additive Manufacturing: Materials, Design, Technologies, and Applications* (Elsevier Ltd, 2017). doi:10.1016/B978-0-08-100433-3.00005-1.

30. López-García, C., García-López, E., Siller, H. R., Sandoval-Robles, J. A. & Rodriguez, C. A. A dimensional assessment of small features and lattice structures manufactured by laser powder bed fusion. *Progress in Additive Manufacturing* **7**, 751–763 (2022).
31. Magarò, P., Alaimo, G., Carraturo, M., Sgambitterra, E. & Maletta, C. A novel methodology for the prediction of the stress–strain response of laser powder bed fusion lattice structure based on a multi-scale approach. *Materials Science and Engineering: A* **863**, 144526 (2023).
32. Sombatmai, A., Uthaisangsuk, V., Wongwiset, S. & Promoppatum, P. Multiscale investigation of the influence of geometrical imperfections, porosity, and size-dependent features on mechanical behavior of additively manufactured Ti-6Al-4V lattice struts. *Mater Des* **209**, 109985 (2021).
33. LIU, W. Optical and XCT Measurement of Additively Manufactured Surfaces. *Fields: journal of Huddersfield student research* **7**, 1–15 (2021).
34. Petrò, S. & Moroni, G. Robustness of geometric verification by segmentation-free X-ray computed tomography. *Procedia CIRP* **92**, 163–168 (2020).
35. Villarraga-Gómez, H. Studies of Dimensional Metrology with X-Ray Cat Scan. *ProQuest Dissertations and Theses* 670 (2018).
36. Schmitt, R. & Niggemann, C. Uncertainty in measurement for x-ray-computed tomography using calibrated work pieces. *Meas Sci Technol* **21**, (2010).
37. A Thompson, I. M. and R. K. L. Measurement Science and Technology X-ray computed tomography for additive manufacturing: a review. (2017).
38. Zanini, F., Sbettega, E. & Carmignato, S. X-ray computed tomography for metal additive manufacturing: Challenges and solutions for accuracy enhancement. *Procedia CIRP* **75**, 114–118 (2018).
39. Aloisi, V. & Carmignato, S. Influence of surface roughness on X-ray computed tomography dimensional measurements of additive manufactured parts. *Case Studies in Nondestructive Testing and Evaluation* **6**, 104–110 (2016).
40. Zanini, F., Sorgato, M., Savio, E. & Carmignato, S. Dimensional verification of metal additively manufactured lattice structures by X-ray computed tomography: Use of a newly developed calibrated artefact to achieve metrological traceability. *Addit Manuf* **47**, 102229 (2021).
41. Nagalingam, A. P., Vohra, M. S., Kapur, P. & Yeo, S. H. Effect of cut-off, evaluation length, and measurement area in profile and areal surface texture characterization of as-built metal additive manufactured components. *Applied Sciences (Switzerland)* **11**, (2021).

42. Le Roux, S., Deschaux-Beaume, F., Cutard, T. & Lours, P. Quantitative assessment of the interfacial roughness in multi-layered materials using image analysis: Application to oxidation in ceramic-based materials. *J Eur Ceram Soc* **35**, 1063–1079 (2015).
43. Zhang, Y., Jung, Y.-G. & Zhang, J. Finite element simulation of residual stress in AM metals. *Multiscale Modeling of Additively Manufactured Metals* 89–107 (2020) doi:10.1016/b978-0-12-819600-7.00006-x.
44. Lopes, A., Rivas, J., Taylor, H., Orquiz, C. & Wicker, R. Measurement systems analysis for beam compensation, scaling factors and geometric dimensioning for a metallic additively manufactured test artifact. *Progress in Additive Manufacturing* (2024) doi:10.1007/s40964-024-00786-8.
45. Cao, X. *et al.* Compression experiment and numerical evaluation on mechanical responses of the lattice structures with stochastic geometric defects originated from additive-manufacturing. *Compos B Eng* **194**, 108030 (2020).
46. Liu, L., Kamm, P., García-Moreno, F., Banhart, J. & Pasini, D. Elastic and failure response of imperfect three-dimensional metallic lattices: the role of geometric defects induced by Selective Laser Melting. *J Mech Phys Solids* **107**, 160–184 (2017).
47. Lane, B., Moylan, S., Yeung, H., Neira, J. & Chavez-Chao, J. Quasi-static position calibration of the galvanometer scanner on the additive manufacturing metrology testbed. (2020).
48. Yeung, H., Neira, J., Lane, B., Fox, J. & Lopez, F. Laser path planning and power control strategies for powder bed fusion systems. *Solid Freeform Fabrication 2016: Proceedings of the 27th Annual International Solid Freeform Fabrication Symposium - An Additive Manufacturing Conference, SFF 2016* 113–127 (2016).
49. Peng, X., Kong, L., An, H. & Dong, G. A Review of In Situ Defect Detection and Monitoring Technologies in Selective Laser Melting. *3D Print Addit Manuf* **10**, 438–466 (2023).
50. Du Plessis, A. *Porosity in Laser Powder Bed Fusion. Fundamentals of Laser Powder Bed Fusion of Metals* (Elsevier Inc., 2021). doi:10.1016/b978-0-12-824090-8.00007-x.
51. Smoqi, Z. *et al.* Monitoring and prediction of porosity in laser powder bed fusion using physics-informed melt pool signatures and machine learning. *Journal of Materials Processing Tech.* **304**, 117550 (2022).